

# The influence of surface roughness on superhydrophobicity

C. Yang,<sup>1,2</sup> U. Tartaglino,<sup>1,3</sup> and B.N.J. Persson<sup>1</sup>

<sup>1</sup>IFF, FZ-Jülich, 52425 Jülich, Germany

<sup>2</sup>International Center for Theoretical Physics (ICTP), I-34014 Trieste, Italy

<sup>3</sup>Democritos National Simulation Center, Via Beirut 2, 34014 Trieste, Italy

Superhydrophobic surfaces, with liquid contact angle  $\theta$  greater than  $150^\circ$ , have important practical applications ranging from self-cleaning window glasses, paints, and fabrics to low friction surfaces. Many biological surfaces, such as the lotus leaf, have hierarchically structured surface roughness which is optimized for superhydrophobicity through natural selection. Here we present a molecular dynamics study of liquid droplets in contact with self-affine fractal surfaces. Our results indicate that the contact angle for nanodroplets depends strongly on the root-mean-square (rms) surface roughness amplitude but is nearly independent of the fractal dimension  $D_f$  of the surface.

The fascinating water repellents of many biological surfaces, in particular plant leaves, have recently attracted great interest for fundamental research as well as practical applications[1, 2, 3, 4, 5, 6, 7, 8]. The ability of these surfaces to make water beads off completely and thereby wash off contamination very effectively has been termed the Lotus effect, although it is observed not only on the leaves of Lotus plant, but also on many other plants such as strawberry, raspberry and so on. Water repellents are very important in many industrial and biological processes, such as prevention of the adhesion of snow, rain drops and fog to antennas, self-cleaning windows and traffic indicators, low-friction surfaces and cell mobility [9, 10, 11].

Most leaves that exhibit strong hydrophobicity have hierarchical surface roughness with micro- and nanostructures made of unwettable wax crystals. The roughness enhances the hydrophobic behavior, so that the water droplets on top tend to become nearly spherical. As a result the leaves have also a self-cleaning property: the rain drops roll away removing the contamination particles from the surface, thanks to the small adhesion energy and the small contact area between the contaminant and the rough leaf[1].

The hydrophobicity of solid surfaces is determined by both the chemical composition and the geometrical micro- or nanostructure of the surface[12, 13, 14]. Understanding the wetting of corrugated and porous surfaces is a problem of long standing interest in areas ranging from textile science [15] to catalytic reaction engineering[16]. Renewed interest in this problem has been generated by the discoveries of surfaces with small scale corrugations that exhibit very large contact angles for water and other liquids—in some cases the contact angle is close to  $180^\circ$ . Such surfaces are referred to as superhydrophobic[17].

The contact angle  $\theta$  between a flat solid surface and a liquid droplet depends on the relation between the interfacial free energies per unit area: solid/liquid  $\gamma_{sl}$ , solid/vapor  $\gamma_{sv}$  and liquid/vapor  $\gamma_{lv}$ . The Young's equation  $\gamma_{sl} + \gamma_{lv}\cos\theta = \gamma_{sv}$ , results from the minimization of the total free energy of the system on a flat substrate surface. Complete wetting corresponds to  $\theta = 0^\circ$ , and

typically happens on solids with high surface energy  $\gamma_{sv}$ . Liquids on low energy surfaces tend to form droplets with high contact angle  $\theta$ .

It is well known that the roughness of a hydrophobic solid (with  $\theta > 90^\circ$  on the flat substrate) enhances its hydrophobicity. If the contact angle of water on such flat solids is of the order of  $100^\circ$  to  $120^\circ$ , on a rough or microtextured surface it may be as high as  $150^\circ$  to  $175^\circ$ [11, 18, 19]. Two distinct models have been proposed to explain this effect. The Wenzel model [20] considers the increase of contact area due to the surface roughness: this leads to an increase of the effective free energy of the solid/liquid interface, making the surface more hydrophobic. The contact angle  $\theta_0$  on the rough surface is obtained from the contact angle  $\theta$  on the microscopically flat surface of the same material through this equation

$$\cos\theta_0 = r\cos\theta \quad (\text{Wenzel model}), \quad (1)$$

where  $r = A/A_0$  is the ratio between the real substrate (area) and the nominal (or projected) area  $A_0$ .

The Cassie model [21] assumes that some air remains trapped between the drop and the cavities of the rough surface. In this case the interface free energy  $\gamma_{sl}$  must be replaced by a weighted average of three interface free energies  $\gamma_{sl}$ ,  $\gamma_{lv}$  and  $\gamma_{sv}$ , with the weights depending on the fraction  $\phi$  of the area where the contact between the liquid and the solid happens. The contact angle is given by

$$\cos\theta_0 = -1 + \phi(1 + \cos\theta) \quad (\text{Cassie model}). \quad (2)$$

Quere et al. state that there exists a critical contact angle  $\theta_c$  such that the Cassie state is favored when  $\theta$  is larger than  $\theta_c$  [22]. For a micro- or nano structured substrate, usually the droplet stays in the Cassie state, but the Cassie state can switch (irreversibly) to the Wenzel state when the droplet is pressed against the substrate [23]. The Wenzel droplets are highly pinned, and the transition from the Cassie to the Wenzel state results in the loss of the anti-adhesive properties generally associated with superhydrophobicity.

Many surfaces in nature, e.g., surfaces prepared by fracture (involving crack propagation), tend to be nearly self-affine fractal. Self-affine fractal surfaces have multiscale roughness, sometimes extending from the lateral size of the surface down to the atomic scale. A self-affine fractal surface has the property that if part of the surface is magnified, with a magnification which in general is appropriately different in the direction perpendicular to the surface as compared to the lateral directions, the surface “looks the same” [24] i.e., the statistical properties of the surface are invariant under this scale transformation.

The most important property of a randomly rough surface is the surface roughness power spectrum defined as [24, 25, 26]

$$C(q) = \frac{1}{(2\pi)^2} \int d^2x \langle h(\mathbf{x})h(\mathbf{0}) \rangle e^{i\mathbf{q} \cdot \mathbf{x}} \quad (3)$$

Here  $h(\mathbf{x})$  is surface height profile and  $\langle \dots \rangle$  stands for ensemble average. We have assumed that the statistical properties of the surface are translational invariant and isotropic so that  $C(q)$  depends only on the magnitude  $q = |\mathbf{q}|$  of the wave vector  $q$ . For a self-affine surface the power spectrum has the power-law behavior  $C(q) \sim q^{-2(H+1)}$ , where the Hurst exponent  $H$  is related to the fractal dimension  $D_f = 3 - H$ . Of course, for real surfaces this relation only holds in some finite wave vector region  $q_0 < q < q_1$ . Note that in many cases there is roll-off wavevector  $q_0$  below which  $C(q)$  is approximately constant. The mean of the square of the roughness profile can be obtained directly from  $C(q)$  using  $\sigma^2 = \langle h^2(\mathbf{x}) \rangle = \int d^2q C(q)$ .

For self-affine fractal surfaces  $r = A/A_0$  is uniquely determined by the root mean square roughness  $\sigma$  and the fractal dimension  $D_f$ . We have[27]

$$A/A_0 = \int_0^\infty dx (1 + x\xi^2)^{1/2} e^{-x} \quad (4)$$

where  $\xi^2 = \int d^2q q^2 C(q)$ . For the surfaces we use in our study, in Fig. 1 we show the ratio  $r = A/A_0$  both as a function of the root mean square roughness  $\sigma$ , and as a function of Hurst exponent  $H$ . As expected,  $A/A_0$  increases with increasing rms-roughness, and decreasing Hurst exponent  $H$  (or increasing fractal dimension  $D_f = 3 - H$ ). Qualitatively, when  $D_f$  increases at fixed rms-roughness, the short wavelength roughness increases while the long wavelength roughness remains almost unchanged.

We have used Molecular Dynamics calculations to study the influence of surface roughness on superhydrophobicity. We have studied hydrocarbon liquid droplets on different self-affine fractal surfaces. The nano-droplet contained 2364 octane molecules  $C_8H_{18}$  at  $T = 300$  K, which is between the melting and boiling points of octane. The fractal surfaces were generated as in Ref. [26]. Different fractal surfaces are obtained by

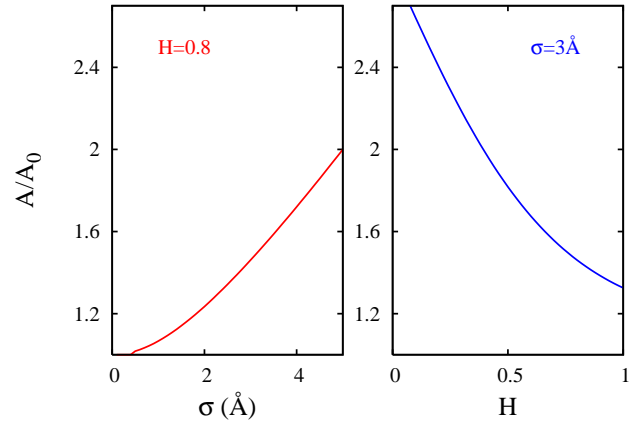


FIG. 1: The ratio  $A/A_0$  between the actual  $A$  and the nominal (or projected)  $A_0$  surface area, as a function of the root mean square roughness  $\sigma$  when Hurst exponent  $H = 0.8$ , and as a function of Hurst exponent  $H$  for  $\sigma = 3 \text{ \AA}$ .

changing the root mean square (rms) roughness amplitude  $\sigma$ , and the fractal dimension  $D_f$ . The roll-off wavevector for the rough surface is  $q_0 = 2\pi/L$  with  $L = 38 \text{ \AA}$ , and the magnitude of the short-distance cut-off wave vector  $q_1 = \pi/a$ , where  $a = 2.53 \text{ \AA}$  is the substrate lattice constant. The (non-contact) cylindrical droplet diameter is about  $104 \text{ \AA}$ , and the size of the droplet-substrate contact area varies from  $\approx 115 \text{ \AA}$  (case (a) in Fig. 2) to  $\approx 60 \text{ \AA}$  (case (c)).

The lubricant molecules are described through the Optimized Potential for Liquid Simulation (OPLS) [28, 29]; this potential is known to provide density and viscosity of hydrocarbons close to the experimental one. We used the Lennard-Jones interaction potential between droplet atoms and substrate atoms. The L-J parameters for a hydrophobic surface are chosen such that the Young contact angle is about  $100^\circ$  when a droplet sits on the flat surface. Because of the periodic boundary condition and the size of our system, the liquid droplet forms a cylinder with the central line along the  $y$ -axis, see Fig. 2. We fit the density profile of the droplet to a cylinder and obtain the contact angle  $\theta = 103^\circ$  as indicated in Fig. 3 for the droplet in contact with the flat substrate.

The apparent contact angle,  $\theta_0$ , as a function of the root mean square roughness (rms), is shown in Fig. 4 with the fractal dimension  $D_f = 2.2$ . There is a strong increase in  $\theta_0$  with increasing rms-roughness amplitude. Fig. 5 shows how  $\theta_0$  depends on the Hurst exponent  $H = 3 - D_f$ . Note that  $\theta_0$  is almost independent of  $H$ .

Accordingly to the Wenzel equation, the apparent contact angle  $\theta_0$  depends only on the surface roughness via the ratio  $r = A/A_0$ . Fig. 1 shows that as  $H$  decreases from 1 to 0.4 (i.e.,  $D_f$  increases from 2 to 2.6),  $A/A_0$  increases by  $\sim 50\%$ . However, the MD-calculations show that the apparent contact angle  $\theta_0$  is almost independent of the fractal dimension, see Fig. 5. Thus the Wenzel

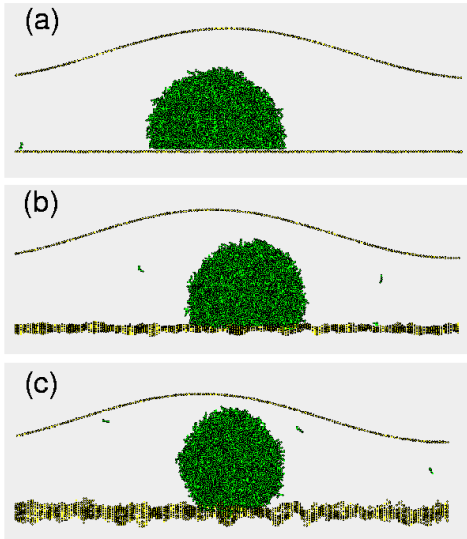


FIG. 2: Snapshots for different root mean square roughness. (a) the droplet is in contact with the flat substrate. (b) and (c) are for rough substrates with the root mean square amplitude  $\sigma = 2.3 \text{ \AA}$  and  $\sigma = 4.8 \text{ \AA}$ , respectively.

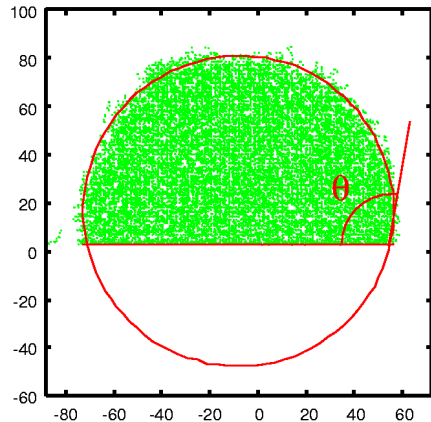


FIG. 3: Determination of the contact angle  $\theta$  for the flat substrate. Side view.

equation cannot be used in the present situation. This is consistent with a visual inspection of the liquid-substrate interface which shows that on the rough substrates, the droplet is “riding” on the asperity tops of the substrate, i.e., the droplet is in the Cassie state. In order to quantitatively verify this, we have calculated the distances  $h(x, y)$  between the bottom surface of the liquid drop and the rough substrate surface in the (apparent) contact area. From the distribution  $P(h)$  of these distances we obtain the fraction  $\psi$  of the (projected) surface area where contact occurs:  $\psi = \int_0^{h_1} dh P(h)$ , where  $h_1$  is a cut-off distance to distinguish between contact and no-contact regions, which has to be comparable to the typical bond distance (we use  $h_1 = 4 \text{ \AA}$ ). Note that due to the thermal fluctuations  $\psi = \psi_0$  for flat surface is

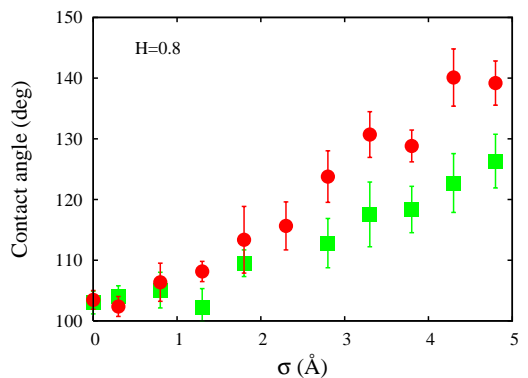


FIG. 4: The contact angle as a function of the root mean square roughness  $\sigma$ . The circle points are numerical results from the simulations, while the square points are obtained from the Cassie model (see Eq. 2). Each data point is an average over several snap-shot configurations. The fractal dimension is  $D_f = 2.2$ .

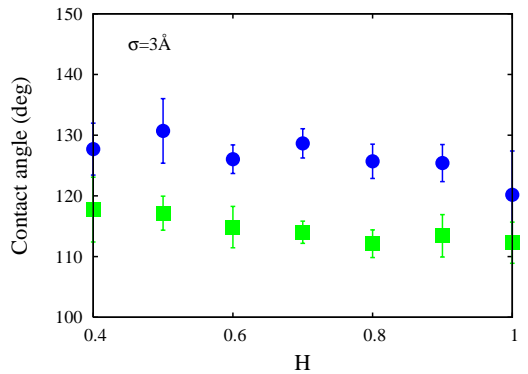


FIG. 5: The contact angle  $\theta$  as a function of Hurst exponent  $H$  for the rms roughness  $\sigma = 3 \text{ \AA}$ . The circles and squares have the same meaning as that in Fig. 4. The fractal dimension is  $D_f = 3 - H$ .

less than 1. Using the normalized  $\phi = \psi/\psi_0$ , the Cassie model predicts the variation of the contact angle with  $\sigma$  and  $H$  given in Fig. 4 and 5 (square points).

Fig. 4 shows that the apparent contact angle  $\theta_0$  increases strongly with increasing rms-roughness amplitude, at fixed fractal dimension  $D_f = 2.2$ , while it is nearly independent of the fractal dimension  $D_f$  (see Fig. 5). Since increasing the fractal dimension at constant rms roughness amplitude mainly increases the short-wavelength roughness, we conclude that the nanoscale wave length roughness doesn't matter so much in determining the contact angle for hydrophobic surfaces, while the long wavelength roughness plays an important role. We attribute this fact to the strong thermal fluctuations in the height (or width)  $h$  of the liquid-solid interface which occur at the nanoscale even for the flat substrate surface. Note also that in our model the wall-wall interaction is long-ranged, decaying effectively

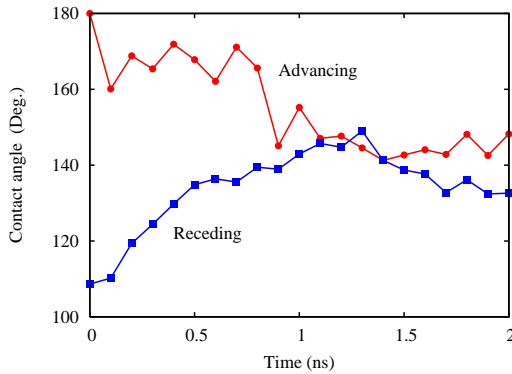


FIG. 6: The Advancing (circles) and receding (squares) contact angle  $\theta$  as a function of time. The thermal equilibrium contact angle has been reached after  $\sim 1$  ns, irrespectively of whether the initial contact angle is larger or smaller than the equilibrium angle.

as  $\sim 1/h^3$ , so there will be a contribution to the interfacial energy also for non-contacting surfaces which, of course, is not rigorously included in the macroscopic Cassie model.

In Fig. 6 we study the hysteresis[14] in the contact angle  $\theta$ . In one case a spherical droplet was attached to the substrate leading to a decrease in the contact angle with increasing time (advancing contact angle). In the other case the droplet was squeezed into a “pancake”-like shape by the upper wall and then released resulting in a contact angle which increases with time (receding contact angle). In both cases, the thermal equilibrium contact angle has been reached after  $\sim 1$  ns. Thus, on *macroscopic* time scales nano-scale roughness will not result in any hysteresis in the contact angle. This is in drastic contrast to simulation studies we have performed (unpublished) for hydrophilic surfaces, where surface roughness results in strong pinning of the boundary line; for such surfaces it is therefore impossible to study (advancing or receding) droplet contact angles (as observed on macroscopic time scales) using molecular dynamics.

Comparing the form of  $P(h)$  for the flat and the most rough surfaces shows that the system is in the Cassie state, but at the nanoscale the difference between the Cassie state and the Wenzel state is not so large due to the thermal fluctuations. This also explain why no hysteresis is observed: The Cassie state is the free energy minimum state and squeezing the droplet into a pancake shape does not push the system permanently into the Wenzel state because even if it would go into this state temporarily, the free energy barrier separating the Cassie and Wenzel states is so small that thermal fluctuations would almost instantaneously kick it back to the (free energy minimum) Cassie state.

In most practical cases it is not possible to modify the surface roughness without simultaneously affecting the chemical nature of the surface. While this is obvious for

crystalline materials, where surface roughening will result in the exposure of new lattice planes with different intrinsic surface energy, it may also hold for amorphous-like materials, where surface roughening may result in a more open atomic surface structure, with an increased fraction of (weak) unsaturated bonds. In our model study a similar effect occurs, and some fraction of the change in the contact angle with increasing root-mean-square amplitude may be associated with this effect. However, the most important result of our study, namely that the contact angle is mainly determined by the long-wavelength roughness, should not be affected by this fact.

To summarize, we have studied the interaction between a liquid hydrocarbon nano-droplets and rough surfaces. The macroscopic contact angle  $\theta_0$  increases with increasing root-mean-square roughness amplitude  $\sigma$  of the surface, but  $\theta_0$  is almost unchanged with increasing fractal dimension  $D_f$ . There is almost no contact angle hysteresis in nanoscale.

This work was partly sponsored by MIUR COFIN No. 2003028141-007 MIUR COFIN No. 2004028238-002, MIUR FIRB RBAU017S8 R004, and MIUR FIRB RBAU01LX5H.

---

- [1] W. Barthlott, C. Neinhuis, *Planta* **202**, 1 (1997)
- [2] C. Neinhuis, W. Barthlott, *Annals of Botany* **79**, 667 (1997)
- [3] A. Otten, S. Herminghaus, *Langmuir* **20**, 2405 (2004)
- [4] See [www.botanik.uni-bonn.de/system/bionik](http://www.botanik.uni-bonn.de/system/bionik) for information involving surface roughness in relation to hydrophobicity and surface self-cleaning in biological systems.
- [5] S. Shibuichi, et. al., *J. Phys. Chem.* **100**, 1996
- [6] R. Blossey, *Nature Mat.* **2** 301, (2003)
- [7] N.A. Patankar, *Langmuir* **20**, 8209 (2004)
- [8] Y.T. Cheng, D.E. Rodak, *Appl. Phys. Lett.* **86** 144101 (2005)
- [9] A. Nakajima, K. Hashimoto, T. Watanabe, *Monatsh. Chem.* **132**, 31 (2001)
- [10] S.R. Coulson, L. Woodward, J.P.S. Badyal, S.A. Brewer, C. Willis, *J. Phys. Chem. B* **104**, 8836 (2000)
- [11] H.Y. Erbil, A.L. Demirel, Y. Avci, O. Mert, *Science* **299**, 1377 (2003)
- [12] R.E. Johnson and R.H. Dettre, *J. Phys. Chem.* **68**, 1744 (1964).
- [13] A. Dupuis and J.M. Yeomans, *Langmuir* **21**, 2624 (2005).
- [14] W. Chen, et. al, *Langmuir* **15**, 3395 (1999).
- [15] M. Suzuki, *Carbon* **32**, 577 (1994)
- [16] T.J. Barton et al, *Chem. Mater.* **11**, 2633 (1999)
- [17] J. Bico, C. Marzolin, D. Quere, *Europhys. Lett.* **47**, 220 (1999)
- [18] S. Herminghaus, *Europhys. Lett.* **52** 165, 2000
- [19] A. Lafuma, D. Quere, *Nature Mat.* **2**, 457 (2003)
- [20] R.N. Wenzel, *Ind. Eng. Chem.* **28**, 988 (1936)
- [21] A.B.D. Cassie, S. Baxter, *Trans. Faraday Soc.* **40**, 546 (1944)
- [22] D. Quere, *Physica A* **313**, 32 (2002)

- [23] G. Carbone, L. Mangialardi, Eur. Phys. J. E. **16** 67, (2005)
- [24] B.N.J. Persson, et. al., J. Phys. Condens. Matter **17**, R1 (2005)
- [25] P.R. Nayak, *ASME J. Lubrication Technology* **93**, 398 (1971)
- [26] C. Yang, U. Tartaglino, B.N.J. Persson, Eur. Phys. J. E. **19** 47, (2006)
- [27] B.N.J. Persson, Eur. Phys. J. E **8**, 385 (2002)
- [28] W.I. Jorgensen, J.D. Madura, C.J. Swenson, J. Am. Chem. Soc. **106**, 6638 (1984)
- [29] D.K. Dysthe, A.H. Fuchs, B. Rousseau, J. Chem. Phys. **112**, 7581 (2000)